Available online at www.sciencedirect.com
SCIENCE DIRECT®
International Journal of Heat and Mass Transfer 47 (2004) 3683–3693
International Journal of HEAT and MASS TRANSFER
www.elsevier.com/locate/ijhmt

The enhancement of steam condensation heat transfer in a horizontal shell and tube condenser by addition of ammonia

Chris Philpott, Joe Deans *

Department of Mechanical Engineering, Engineering Building, University of Auckland, 20 Symonds Street, Private Bag, Auckland 192019, New Zealand

Received 22 May 2003; received in revised form 1 April 2004

Abstract

This paper reports on the rates of condensation heat transfer for weak ammonia–water mixtures in a horizontal, shell and tube condenser. It is shown that for inlet ammonia concentrations in the range 0.2–0.9 wt.% the average condensation heat transfer for the condenser was enhanced by up to 14%. Furthermore, local enhancement of the condensation heat transfer of up to 34% occurred at local bulk vapour concentrations between 0.2 and 2 wt.% ammonia. This enhancement was caused by the Marangoni effect which produced a disturbed, turbulent banded condensate film and a corresponding drop in the thermal resistance of the condensate film.

1. Introduction

The general conclusion of previous binary mixture condensation studies has been that binary mixture condensation occurs at a lower heat transfer rate than pure vapour condensation. This lower heat transfer rate has been attributed to the development of a mass diffusion layer between the bulk vapour and the surface of the condensate film that acts as an additional resistance to heat transfer [1]. Although this deleterious effect can be reduced by high thermal gradients, large vapour velocities and finned tubes [2], the reduced heat transfer associated with binary mixture condensation has, until recently, been accepted as largely unavoidable.

It is notable, however, that this conclusion was reinforced by numerical studies where the condensate film was assumed to be smooth and laminar. While such a condition readily facilitates modelling of the binary mixture condensation problem, it ignores the potential of binary mixtures to exhibit condensation behaviour not possible with pure vapours. In particular, the condensation of binary mixtures can be significantly influenced by the Marangoni effect. This effect describes the influence of surface tension gradients, which can develop in liquid mixtures from local perturbations in concentration and temperature.

The Marangoni effect has been observed in several heat and mass transfer processes such as distillation and condensation [3–6]. In condensation the commonly accepted criteria used to determine the stability of the condensate film to surface tension driven effects was developed by Ford and Missen [7] who concluded that the condition for instability could be expressed by Eq. (1). The criterion states that if the change in surface tension with respect to film thickness is positive, the film will tend to be unstable. This conclusion is self evident when a small area of disturbed film is considered. If a region of this film that has the greatest depth also has the highest surface tension, then condensate will be drawn from adjacent thin film regions with lower surface tension and the original disturbance to the film will be reinforced. It was also shown that the inequalities expressed in Eq. (1) could be evaluated as a product of two terms derived from the properties of the mixture and the nature of the process. Two forms of this relation are given in Eqs. (2a) and (2b).

* Corresponding author. Tel.: +64-9-373-7599; fax: +64-9-373-7479.
E-mail address: j.deans@auckland.ac.nz (J. Deans).

0017-9310/$ - see front matter © 2004 Elsevier Ltd. All rights reserved.
doi:10.1016/j.ijheatmasstransfer.2004.04.008

Nomenclature

A	area (m^2)
a	factor a in Ackermann correction (Eq. (8)) ($NC_{p,v}/h_v$)
C_p	specific heat at constant pressure (kJ/kg K)
c	molar concentration (mol/m^3)
D_{12}	diffusion coefficient (m^2/s)
g	gravitational acceleration (m/s^2)
h	heat transfer coefficient (W/m^2 K)
h_{fg}	latent heat of condensation (kJ/kg)
j	molar flux (relative to average flux) (mol/m^2 s)
Ja	modified liquid Jacob number $[C_p(T_i - T_{w,o})/h_{fg}]$
k	thermal conductivity (W/m K)
k_{ss}	thermal conductivity of stainless steel (W/m K)
L	length of tube section (m)
$\dot{n}$	molar flux relative to fixed axes (mol/m^2 s)
N	molar flow rate (mol/s)
Pr_l	Prandtl number of condensate film $[C_p\mu_l/k_l]$
Q	total heat transfer (W)
q	heat flux (W/m^2)
R	thermal resistance (K/W)
R_{tc}	thermal resistance of tube wall to thermocouple (K/W)
$r_{w,o}$	tube outside wall radius (m)
r_{tc}	tube thermocouple radius (m)
Re	Reynolds number of condensate film $[4\Gamma/\mu_l]$
T	temperature (K)
wt.%	weight percent
x	mass fraction of the more volatile species in the condensate

Greek symbols

σ	surface tension (N/m)
δ	film thickness (M)
ρ	density (kg/m^3)
μ	viscosity (N s/m^2)
ω	molar fraction (mol/mol)
Γ	mass flow rate of condensate per unit length tube (kg/m s)

Superscripts and subscripts

–	average
∞	bulk condition
cw	cooling water
i	interface
l	liquid
lv	latent heat
Nu	according to Nusselt theory
o	outside
s	sensible heat
tc	thermocouple
v	vapour
w	wall

$$\frac{\partial\sigma}{\partial\delta} > 0 \quad \text{(unstable condensate film)} \tag{1}$$

$$\frac{\partial\sigma}{\partial\delta} = \left(\frac{\partial\sigma}{\partial T}\right)_{sat} \cdot \frac{\partial T}{\partial\delta} \tag{2a}$$

$$\frac{\partial\sigma}{\partial\delta} = \left(\frac{\partial\sigma}{\partial x}\right)_{sat} \cdot \frac{\partial x}{\partial\delta} \tag{2b}$$

During the condensation processes, $\partial T/\partial\delta$ is positive, while $\partial x/\partial\delta$ is negative. The stability of the film is therefore dependent on the nature of the mixture. If the more volatile component has the lower surface tension, and if the mixture surface tension does not exhibit some minimum or maximum at an intermediate concentration, then the condensate film will tend to become unstable. The presence of such a maximum or minimum would serve to complicate the description of the system because they imply the possibility of both positive and negative behaviour in the same system. The perturbation of the liquid film and the resulting flows within the film caused by the Marangoni effect are shown schematically in Fig. 1.

Recent research has identified that the Marangoni effect will generate non-smooth condensate films that

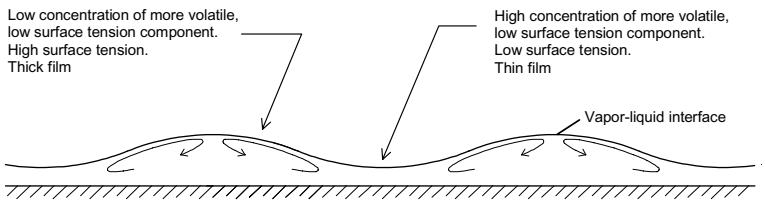

Fig. 1. Schematic of film instabilities caused by the Marangoni effect showing the resulting convection cells within the condensate film and the increased interfacial heat transfer area.

range from 'pseudo droplet' [6,8] to 'ringwise' [9] morphologies. This non-smooth behaviour has been shown to significantly reduce the condensate film heat transfer resistance; however this effect has been outweighed by the increased resistance of the vapour diffusion layer. It was in this context that Morrison and Deans [10] published research showing that at very low concentrations of ammonia, steam condensation heat transfer on a short, horizontal tube was actually enhanced by up to 13%. This enhancement was attributed to the Marangoni effect which produced a disturbed condensate film at ammonia concentrations where the diffusion layer resistance remained low. This paper extends the work of Morrison and Deans [10] by investigating the condensation of weak ammonia–water mixtures in a simple, horizontal shell and tube condenser.

2. Experimental method

The test condenser consisted of a 700 mm long, 150 mm diameter, stainless steel shell and a horizontal, 20 mm diameter, stainless steel tube arranged in a counter-flow, single tube and shell pass configuration. The shell (vapour) side was divided into six sections by a series of baffles, which produced an approximately cross-flow vapour flow pattern. Vapour composition, temperature and pressure could be measured at several points along the condenser shell and sight glasses allowed the condensation process to be observed visually. The tube was instrumented with three thermocouples embedded in the tube wall along the length of the tube and could be rotated through 360°, facilitating radial tube surface temperature measurements. Thermistors positioned along the length of a twisted tape insert inside the tube measured the temperature of the cooling water, which combined with the cooling water flow rate provided an estimate of the energy transferred to each section of the condenser tube. A schematic diagram of the test condenser showing its major components and general dimensions together with the flow path of the vapour and condensate is shown in Fig. 2. It should also be noted that except for small amounts of vapour that were purged prior to each test to remove any non-condensable gas, all of the vapour entering the test condenser was condensed, i.e. the condenser operated as a total condenser.

The tube wall temperature in condenser sections 2, 4 and 6 (see Fig. 2) was measured at 30 degree intervals around the circumference of the tube. The average outside tube surface temperature ($\overline{T}_{w,o}$) for each of these sections was then calculated using the corresponding average tube wall temperature ($\overline{T}_{w}$), the cooling water energy balance (Q_{cw}) and an estimate of the thermal resistance ($R_{tc,w}$,) between the tube wall thermocouple and the tube surface (Eq. (3a)). Finally, the average condensation heat transfer coefficients ($\bar{h}_{w,o}$) for sections 2, 4 and 6 of the condenser tube were calculated using Eq. (4). This method was verified by the excellent agreement of the experimental results for pure steam condensation with Nusselt's theory [11]. Furthermore, a worst case error analysis, based on the errors presented in Table 1, suggested that the maximum experimental error associated with the condensation heat transfer coefficient results was less than 6%.

$$\overline{T}_{w,o} = \overline{T}_{tc} + Q_{cw} \cdot R_{tc} \tag{3a}$$

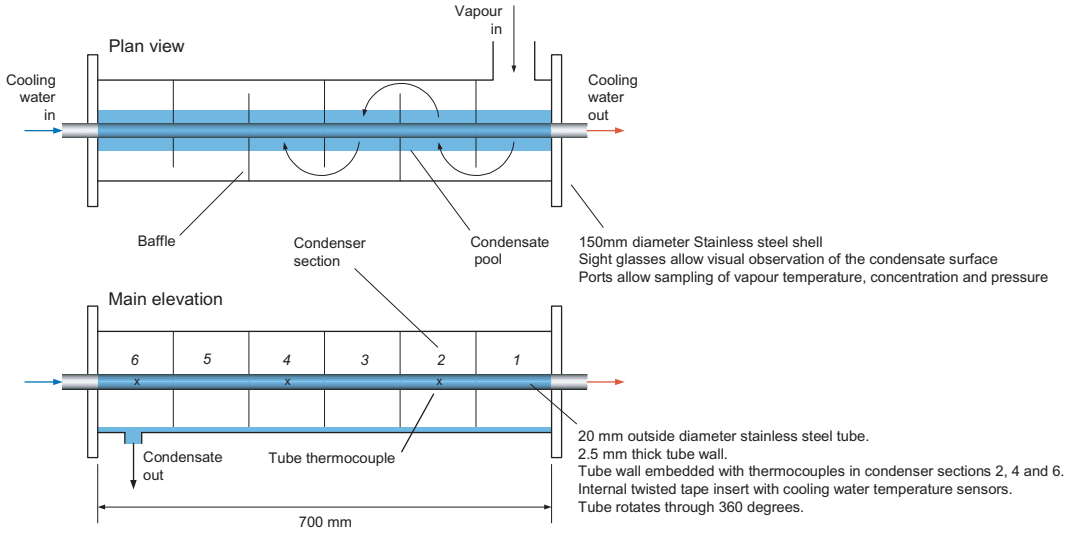

Fig. 2. Schematic diagram of the ammonia–water test condenser.

Table 1
Potential measurement errors

Thermocouples (K type)	±0.2 °C
Thermistors (precision glass encapsulated)	±0.02 °C
Cooling water flow rate (Rotameter)	±0.0038 kg/s (1% of full scale)
Ammonia concentration (titration)	±3% of measurement

$$\text{where } R_{tc} = \frac{\ln\left(\frac{r_{w,o}}{r_{tc}}\right)}{2 \cdot \pi \cdot k_{ss} \cdot L} \tag{3b}$$

$$\bar{h}_{w,o} = \frac{Q_{cw}}{A_{w,o} \cdot (T_{v,\infty} - \overline{T}_{w,o})} \tag{4}$$

The experimental condensation heat transfer coefficients were compared to both Nusselt's theory of condensation (Eq. (5)) and a numerical binary condensation model. The theoretical results from Eq. (5) were calculated for pure steam condensing on the tube surface with the vapour at the same saturation temperature as that of the binary vapour and a uniform outside wall temperature equal to the experimental average outside wall temperature.

$$\bar{h}_{Nu} = 0.728 \cdot \left(\frac{k_l^3 \cdot g \cdot \rho_l \cdot (\rho_l - \rho_v) \cdot h_{fg}}{\mu_l \cdot (T_{v,\infty} - \overline{T}_{w,o})} \right)^{0.25} \tag{5}$$

3. Model

The one dimensional model was based on the geometry of the test condenser and the binary condensation theory of Colburn and Drew [12]. Colburn and Drew considered the 'point' or initial condensation of miscible binary vapours on a vertical surface. Their model assumed that mass transfer existed only in the direction normal to the vapour–liquid interface and implied that the composition of the condensate was determined by condensation at that point alone. Furthermore, they postulated that at the vapour–liquid interface, the local liquid and vapour compositions could be approximated by static equilibrium conditions. Using a vapour side diffusional mass transfer resistance derived from Ficks law (Eq. (6)) together with the boundary conditions for the vapour film implied by the assumption of static equilibrium at the interface, Eq. (7) was derived. To complete the model, the actual heat transfer had to be quantified. The total heat transfered contains both the sensible cooling of the vapour and the latent heat of condensation. This energy balance is given by Eq. (8), which includes the Ackermann correction [13]. The heat transfer associated with the condensation process, given by Eq. (8), was then equated with the heat transfer coefficient of the condensate film. This is described by Eq. (9). The temperature and composition at the vapour–liquid interface could then be determined by iteration of Eqs. (8) and (9).

$$j_i = c_v D_{12} \nabla \omega_l \tag{6}$$

$$\dot{n} = \frac{D_{12} c_v}{\delta_v} \cdot \ln \left| \frac{\frac{\dot{N}_l}{\dot{N}} - \omega_{v,\infty}}{\frac{\dot{N}_l}{\dot{N}} - \omega_{v,i}} \right| \tag{7}$$

$$\begin{aligned} q &= q_s + q_{lv} \\ &= h_v \cdot (T_{v,\infty} - T_i) \cdot \left[\frac{a}{1 - e^{-a}} \right] + h_{fg} \cdot \frac{D_{12} c_v}{\delta_v} \\ &\quad \cdot \ln \left| \frac{\frac{\dot{N}_l}{\dot{N}} - \omega_{v,\infty}}{\frac{\dot{N}_l}{\dot{N}} - \omega_{v,i}} \right| \end{aligned} \tag{8}$$

$$q = h_l \cdot (T_i - T_{w,o}) \tag{9}$$

It should be noted that currently there is no complete theory to predict the heat transfer coefficients of disturbed binary condensate films. The model therefore predicted the condensate film heat transfer coefficient using Nusselt's theory, which presumes a smooth, laminar condensate film. This approach highlighted the difference between smooth and non-smooth binary condensate film behaviour.

A full description of the model together with further details of the experimental apparatus and procedures is given by Philpott [14].

4. Results and discussion

All of the ammonia–water condensation experiments were carried out at the same cooling water flow rate (0.25 kg/s), cooling water inlet temperature (14 °C) and condenser heat load (7.3 kW). The cooling water temperature increase from condenser inlet to outlet was therefore approximately 7 °C. The tests were characterised by relatively low bulk vapour velocities and Reynolds numbers. Vapour velocities within the condenser ranged from near static to 0.6 m/s, producing vapour Reynolds numbers, based on tube diameter, between 30 and 400. The ammonia–water condensation tests were also characterised by moderate liquid Prandtl numbers, $2 < Pr_l < 5$, low modified liquid Jacob numbers, $0.02 < Ja_l < 0.04$ and relatively low liquid Reynolds numbers, $20 < Re_{D,l} < 60$ (all based on mixture properties described in Appendix A). While the tests were concerned with the condensation of mixtures rather

than pure vapours, the non-dimensional numbers listed above indicate that Nusselt's analysis could be applied to the condensate film without consideration of interfacial shear stress, inertial forces and energy convection.

Furthermore, the ammonia–water condensation tests were conducted at average outside wall temperatures significantly below the bubble point of the mixture (>5 °C). This indicated that local total condensation occurred along the length of the tube in all of the tests. However, the pool of condensate in the bottom of the condenser tended to re-establish equilibrium with the bulk vapour, producing an increase in the bulk vapour ammonia concentration from vapour inlet to condensate outlet.

Due to the ammonia concentration gradient which developed within the condenser a range of condensate film behaviour was observed along the length of the condenser tube in each of the ammonia water condensation tests. The tests began at low inlet vapour ammonia concentrations (0.2 wt.%) and progressed to higher concentrations (1.6 wt.%). Initially the condensate film behaviour ranged from smooth at the vapour inlet end of the condenser where the ammonia concentration was low, to slightly disturbed at the bottom of the tube in the middle of the condenser, to part smooth, part banded at the condensate outlet end of the condenser where the ammonia concentration was at its highest. It should be noted that the films described as smooth in the ammonia water tests were not as disturbance free as those found in the steam tests but displayed the odd random ripple. These disturbances were not stable but would spontaneously appear and disappear.

When the inlet ammonia concentration was increased the condensate film became increasingly disturbed. Fig. 3 shows the condensate film observed at the condensate outlet end of the condenser (section 6) during an ammonia water condensation test with an inlet vapour concentration of 0.47 wt.% ammonia. The film was highly disturbed, displaying thin, fast moving turbulent bands and also showed signs of pseudo-droplet condensation. This film behaviour corresponds to some of the lowest condensate film resistances measured (see Fig. 10 for details). In the earlier stages of the condenser the condensate film was part smooth, part turbulent banded. These film disturbances developed from right to left on the tube surface (see Fig. 4a and b), the reason for this behaviour is unclear but may have been due to tube surface temperature effects. The cooling water inside the tube flowed from left to right and was slightly warmer (1–2 °C) towards the right of any given condenser section. This would have produced a slightly higher tube surface temperature and lower vapour to outside tube wall temperature difference on the right hand side of the condenser section. As noted by Tamir [15] lower vapour to wall temperature differences tend to promote film disturbances during binary mixture condensation and it is therefore likely that disturbances in the condensate film would begin to develop where the vapour to wall temperature difference was lowest, namely the right hand side of each section of the condenser.

Fig. 3. Turbulent banded condensate film on condenser tube surface. Local bulk vapour concentration = 1.09 wt.% ammonia. Vapour to average outside wall temperature difference = 10.5 °C.

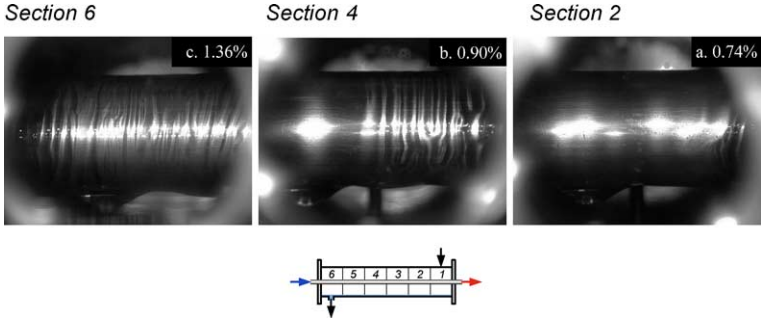

Fig. 4. (a–c) The condensate film at various positions within the condenser. (Inlet vapour ammonia concentration 0.55 wt.%, local bulk vapour ammonia concentration inset.)

With further increases in the inlet vapour ammonia concentration the film disturbances eventually developed over the entire tube surface. However, at these relatively high ammonia concentrations the banded structure of the film was thicker and far less vigorous than that observed at lower vapour concentrations.

The local experimental condensation heat transfer coefficients are presented in Figs. 5 and 6. It can be seen that the experimental results for pure steam agree well with both Nusselt's theory (Eq. (5)) and the numerical model. Furthermore, Figs. 5 and 6 show an enhancement in the condensation heat transfer coefficient for condenser sections 4 and 6 between vapour concentrations of approximately 0.3–2 wt.% ammonia, with a maximum enhancement of approximately 80% over the binary condensation model and 34% over the Nusselt

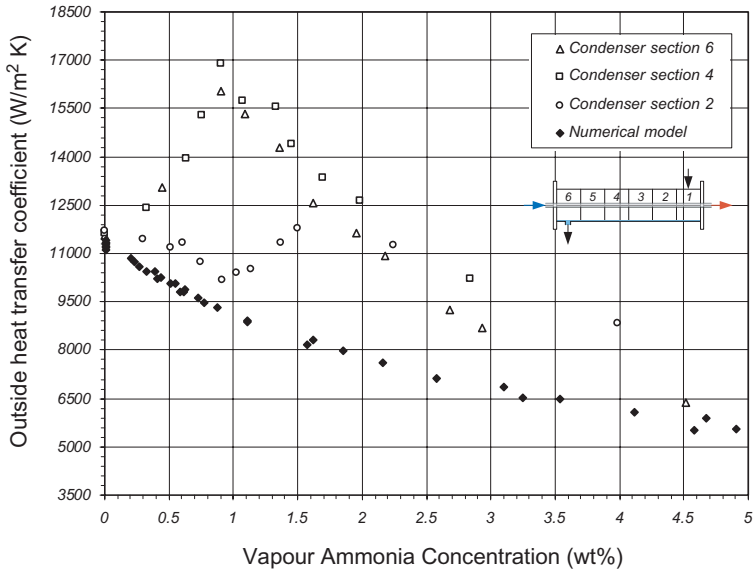

Fig. 5. Sectional condensation heat transfer coefficients.

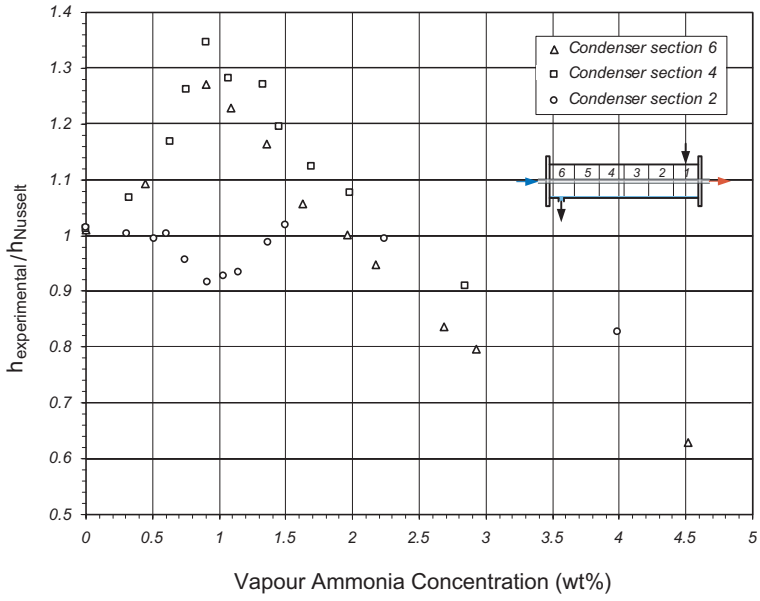

Fig. 6. Ratio of the sectional condensation heat transfer coefficient to Nusselt theory (Eq. (5)).

prediction occurring at an ammonia concentration of 0.9 wt.%. It can also be seen that for local bulk vapour ammonia concentrations greater than 2 wt.% the condensation heat transfer coefficient was less than that predicted for pure steam, decreasing with increasing ammonia concentration as predicted by the model. This trend is consistent with previous binary condensation research [1,12].

Figs. 5 and 6 also show that the heat transfer coefficient for section 2 of the condenser tube generally remained at or below the Nusselt prediction and initially decreased in a similar fashion to that predicted by the binary condensation model. This was caused by a delay in the axial growth of disturbed film in the early sections of the condenser. Condensate film disturbances were present in section 2 at these ammonia concentrations; however they were restricted to the right hand side of the tube (see Fig. 4a for example) and therefore did not influence the thermocouple embedded in the tube wall near the centre of the section. This produced an underestimate in the average tube surface temperature of the condenser section and hence an underestimate of the average condensation heat transfer coefficient. Thus, due to the geometry of the instrumentation, the experimental results tended to exaggerate the seeming lack of disturbances in section 2 of the condenser. Nevertheless, the reasons why the development of condensate film disturbances were retarded in the early sections of the condenser at vapour concentrations and coolant temperatures similar to those found in the later stages of the condenser remains unknown. If anything, the above discussion highlights the sensitivity of the onset of Marangoni instabilities to experimental parameters during binary condensation. The onset of Marangoni disturbances is the focus of research being conducted by Korte et al. [16,17].

Figs. 7 and 8 present the overall tube condensation heat transfer coefficients at various vapour inlet concentrations. The values were calculated by averaging the sectional heat transfer coefficients on a tube area basis. A maximum overall increase in the condensation heat transfer coefficient of approximately 40% over the binary condensation model and 14% over the Nusselt prediction occurred at an inlet vapour ammonia concentration of 0.47 wt.%. The enhancement of the overall condensation heat transfer coefficient was reflected in the condenser pressure, shown in Fig. 9.

The increased heat transfer for the ammonia–water condensation tests was a result of the disturbed condensate film induced by the Marangoni effect. Since the tests were conducted under conditions of local total condensation, i.e. the vapour–liquid interface temperature could be assumed to be at the bubble point temperature of the mixture, it was possible to isolate the thermal resistances of the vapour and condensate films (Eqs. (10) and (11), respectively) from the overall condensation resistance (Eq. (12)).

$$R_{\mathrm{v}} = \frac{(T_{\mathrm{v}} - T_{\mathrm{i}})}{Q} \tag{10}$$

$$R_{\mathrm{l}} = \frac{(T_{\mathrm{i}} - T_{\mathrm{w,o}})}{Q} \tag{11}$$

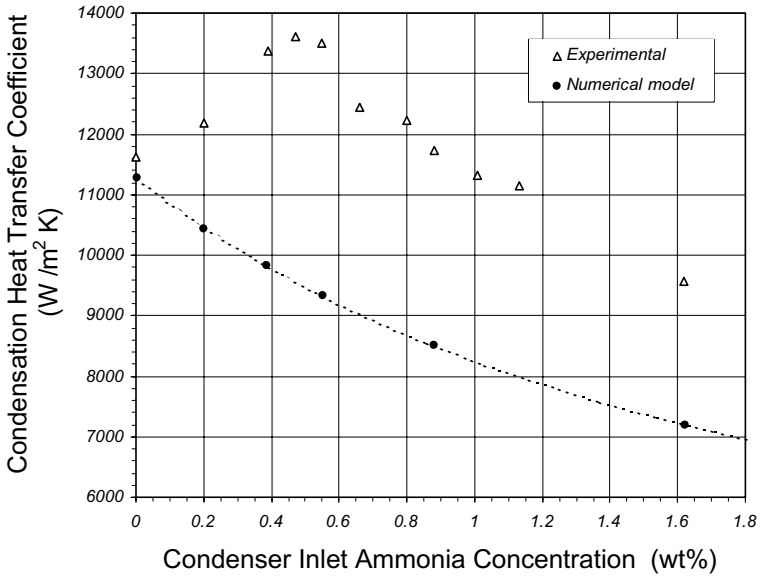

Fig. 7. Overall tube condensation heat transfer coefficient.

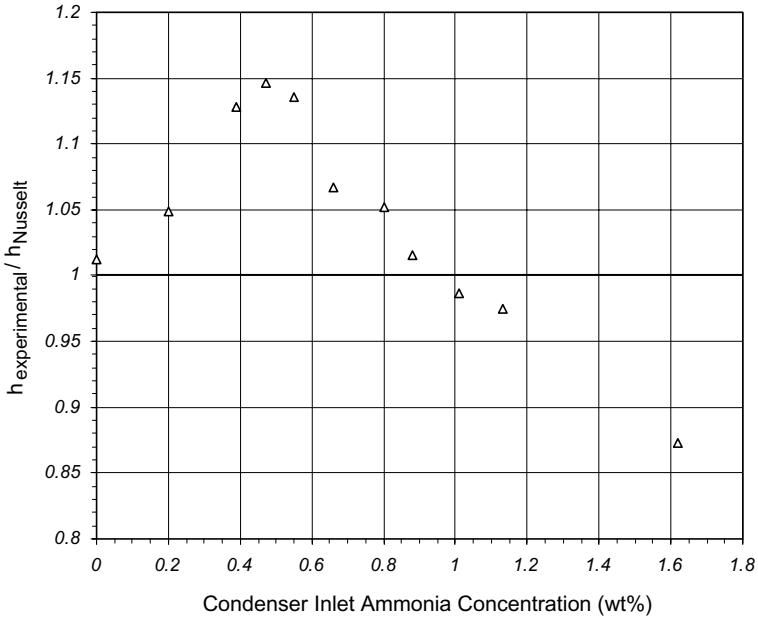

Fig. 8. Ratio of overall condensation heat transfer coefficient to Nusselt's prediction.

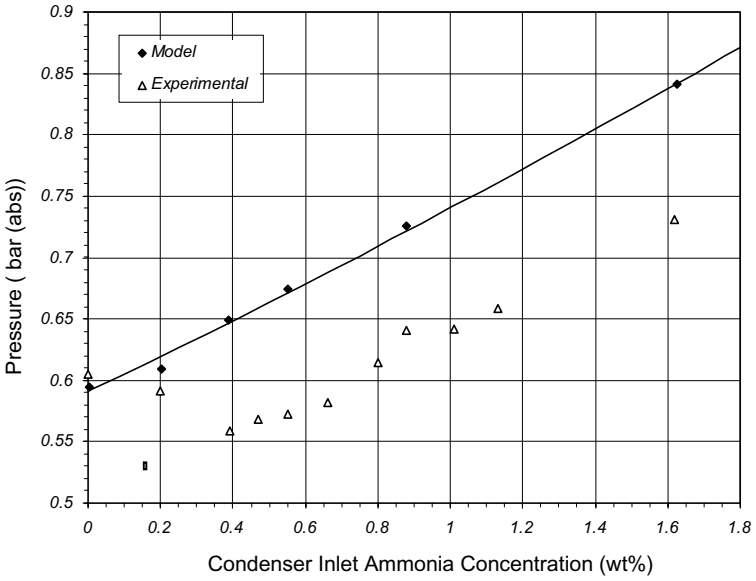

Fig. 9. Condenser pressure variation with inlet vapour ammonia concentration.

$$R_o = \frac{(T_v - T_{w,o})}{Q} \tag{12}$$

Fig. 10 shows that the resistance of the vapour film was relatively low at low ammonia concentrations and generally increased with increasing concentration. This behaviour was consistent with that predicted by the binary mixture condensation model. At very low ammonia concentrations (<0.5 wt.%) the thermal resistance of the condensate film was also similar to that predicted by the model. However, as the ammonia concentration was increased and the film disturbances

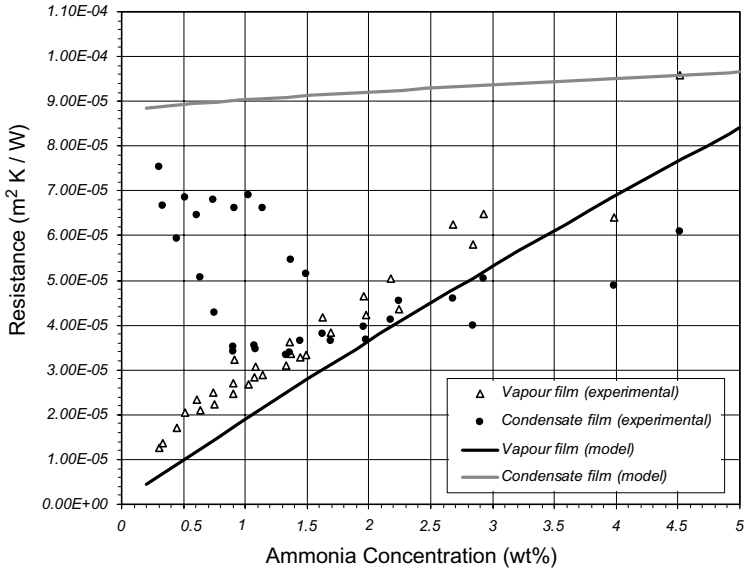

Fig. 10. Vapour and condensate film resistances.

became more vigorous the condensate film resistance was markedly reduced, with minimum resistances corresponding to turbulent banded condensate films similar to that shown in Fig. 3. Further increases in the ammonia concentration (>2 wt.%) generally produced slightly less vigorous condensate film behaviour and higher condensate film resistances.

Fig. 11 compares the heat transfer through the actual, disturbed condensate film with that theoretically predicted for a smooth, laminar binary condensate film. It can be seen that at low ammonia concentrations where the condensate film was relatively smooth the ratio of the experimental to theoretical heat transfer tended towards unity. As the disturbances increased in

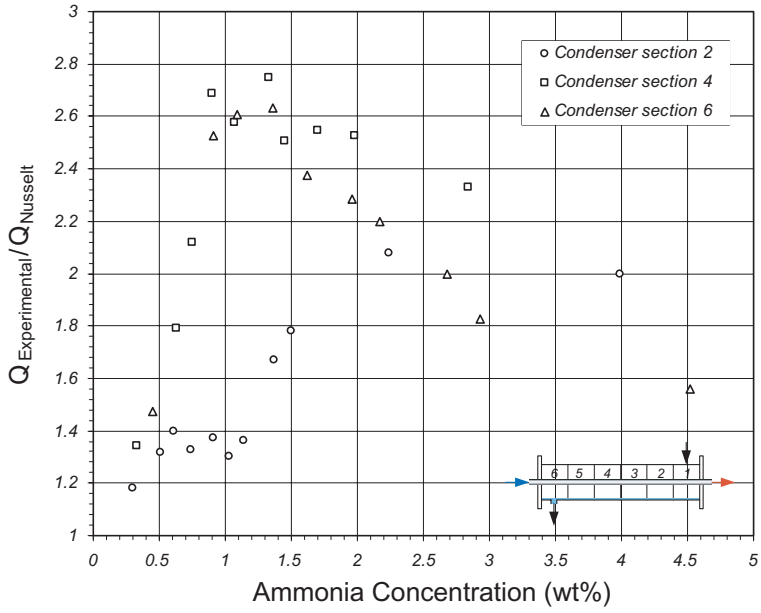

Fig. 11. Condensate film heat transfer enhancement.

intensity the heat transfer through the condensate film also increased, with a maximum enhancement of 175% occurring at an ammonia concentration of approximately 1.3 wt.%, which is significantly greater than the 32% enhancement of the condensate film heat transfer reported by Morrison and Deans [10]. This greater enhancement is believed to be due to the more vigorous nature of the condensate film disturbances reported in this paper. Further increases in the ammonia concentration generally decrease the heat transfer though the condensate film, however some enhancement was still evident at a concentration of 4.5 wt.% ammonia.

5. Conclusions

The results show that for the condensation of weak ammonia–water mixtures on a horizontal tube the condensate film is generally disturbed. These film disturbances were caused by the Marangoni effect i.e. surface tension gradients within the condensate film. The film disturbances caused the heat transfer through the condensate film to increase by as much as 175%. However, this heat transfer enhancement was partially off set by the added thermal resistance of the vapour film, producing local condensation heat transfer coefficients up to 34% higher than that predicted for pure steam. Furthermore, it was shown that for inlet ammonia concentrations in the range 0.2–0.9 wt.% the average condensation heat transfer for the entire condenser was enhanced by up to 14%.

Appendix A. Property data

All condensate film property data was evaluated at the liquid film temperature and composition, T_l and x_l, respectively. The average liquid film temperature was estimated using Eq. (A.1), while the ammonia concentration of the condensate film was taken to be equal to the interface concentration, i.e. $x_l = x_i$

$$T_l = T_{w,o} + 0.5 \cdot (T_i - T_{w,o}) \tag{A.1}$$

The dynamic viscosity of the condensate film, (μ_l) was estimated using a correlation by Morrison [18] fitted to experimental data from Vemura [19]. The correlation was in the form of a mass averaged value and a correction based on the difference between the viscosity values of the pure components.

$$\mu_l = \left(x_i \cdot \mu_{l,NH_3} + (1 - x_i) \cdot \mu_{l,H_2O}\right) + \left(\left(\mu_{l,H_2O} - \mu_{l,NH_3}\right) \cdot f(x_i) \cdot f(T)_l\right) \tag{A.2}$$

where

$$f(x_i) = 4.00175 \cdot x_i - 10.4785 \cdot x_i^2 + 7.88742 \cdot x_i^3 - 1.39324 \cdot x_i^4 \tag{A.3}$$

and

$$f(T_l) = \frac{0.8047 - 0.005423 \cdot T_l}{0.526} \tag{A.4}$$

The thermal conductivity of the condensate film (k_l) was estimated from Lucas [20].

$$k_l = \frac{1}{\sqrt{x_i \cdot k_{l,NH_3}^{-2} + (1 - x_i) k_{l,H_2O}^{-2}}} \tag{A.5}$$

All vapour side properties were evaluated at the average vapour mixture film temperature and concentration, T_v and y_v ([21]).

$$T_v = \frac{T_i + T_\infty}{2} \tag{A.6}$$

$$y_v = \frac{y_i + y_\infty}{2} \tag{A.7}$$

According to Lucas [20] the specific heat of the gas mixture ($C_{p,v}$) can be estimated on a mass fraction basis from the values of the pure components.

$$C_{p,v} = y_v \cdot C_{p,v,NH_3} + (1 - y_v) \cdot C_{p,v,H_2O} \tag{A.8}$$

The viscosity of the vapour mixture (μ_v) can be estimated from Liley et al. [22].

$$\mu_v = \frac{y_v \cdot \mu_{v,NH_3}}{y_v + (1 - y_v) \cdot \Theta_{12}} + \frac{(1 - y_v) \cdot \mu_{v,H_2O}}{y_v \cdot \Theta_{21} + (1 - y_v)} \tag{A.9}$$

where

$$\Theta_{12} = \frac{\left(1 + \left(\mu_{v,NH_3}/\mu_{v,H_2O}\right)^{1/2} \cdot \left(\widetilde{M}_{H_2O}/\widetilde{M}_{NH_3}\right)^{1/4}\right)^2}{\left(8 \cdot \left(1 + \widetilde{M}_{NH_3}/\widetilde{M}_{H_2O}\right)\right)^{1/2}} \tag{A.10}$$

and

$$\Theta_{21} = \left(\mu_{v,H_2O}/\mu_{v,NH_3}\right) \cdot \left(\widetilde{M}_{NH_3}/\widetilde{M}_{H_2O}\right) \cdot \Theta_{12} \tag{A.11}$$

The thermal conductivity of the gas mixture (k_v) can be calculated in a similar manner Lucas [20].

$$k_v = \frac{y_v \cdot k_{v,NH_3}}{y_v + (1 - y_v)} + \frac{(1 - y_v) \cdot k_{v,H_2O}}{y_v \cdot \Theta_{21} + (1 - y_v)} \tag{A.12}$$

where Θ_{12} and Θ_{21} are calculated using Eqs. (A.10) and (A.11) with μ_{v,NH_3} and μ_{v,H_2O} replaced by k_{v,NH_3} and k_{v,H_2O}, respectively.

All other property data including mixture dew and bubble points, equilibrium ammonia concentrations, latent heats of vapourisation, and liquid and vapour mixture densities were calculated using an Ammonia Water Mixtures (AWMix) library module. AWMix is a procedure compiled into a dynamic-link-library for use with the Engineering Equation Solver program produced by F-Chart Software. The module is an imple-

mentation of the Helmholtz free energy model for water-ammonia-mixtures established by Tillner-Roth and Friend [23], based on the equation of state for pure water established by Pruß and Wagner [24], and the equation of state for pure ammonia by Tillner-Roth [25]. This formulation offers a consistent description of all thermodynamic properties of the mixture.

References

[1] K. Stephan, Heat Transfer in Condensation and Boiling, Springer-Verlag, Berlin, 1992.

[2] K. Hijikata, N. Himeno, S. Goto, Forced convective condensation of a binary mixture of vapours, JSME Int. J. 30 (1987) 1951–1956.

[3] F.J. Zuiderweg, A. Harmens, The influence of surface phenomena on the performance of distillation columns, Chem. Eng. Sci. 9 (1958) 89–103.

[4] G.S. Bainbridge, H. Sawistowski, Surface tension effects in sieve plate distillation columns, Chem. Eng. Sci. 19 (1964) 992–993.

[5] V.V. Mirkovich, R.W. Missen, Non-filmwise condensation of binary vapours of miscible liquids, Can. J. Chem. Eng. 39 (1961) 86–87.

[6] V.V. Mirkovich, R.W. Missen, A study of the condensation of binary vapours of miscible liquids. II: heat transfer coefficients for filmwise and non-filmwise condensation, Can. J. Chem. Eng. 41 (1963) 73–78.

[7] J.D. Ford, R.W. Missen, On the conditions for stability of falling films subject to surface tension disturbances; the condensation of binary vapours, Can. J. Chem. Eng. 46 (1968) 309–312.

[8] K. Hijikata, T. Fukasaku, O. Nakabeppu, Theoretical and experimental studies on the microstructure of pseudo-dropwise condensation of a binary mixture, in: Proceedings of the 1994 Int. Mech. Engng. Congress and Exposition, ASME-HTD, Chicago, vol. 291, 1994, pp. 57–62.

[9] M. Goto, T. Fujii, Film condensation of binary refrigerant vapours on a horizontal tube, in: Proceedings of the 7th International Heat Transfer Conference, Munich, vol. 5, 1982, pp. 71–76.

[10] J.N.A. Morrison, J. Deans, Augmentation of steam condensation heat transfer by addition of ammonia, Int. J. Heat Mass Transfer 40 (1997) 765–772.

[11] W. Nusselt, Die oberflachenkondensation des wasser dampfes, Z. Ver. Deut. Inineure 60 (1916) 541–575.

[12] A.P. Colburn, T.B. Drew, The condensation of mixed vapors, Trans. AIChE 33 (1937) 197–212.

[13] G. Ackermann, Wärmeübergang und molekulare Stoffübertragung im gleichen Feld bei großen Temperatur- und Partialdruckdifferenzen, VDI Forschungsheft 382 (1937) 1–16.

[14] C. Philpott, The condensation of ammonia–water mixtures in a horizontal shell and tube condenser, Ph.D. thesis, University of Auckland, New Zealand, 2003.

[15] A. Tamir, Mixed pattern condensation of multicomponent mixtures, Chem. Eng. J. 17 (1979) 141–156.

[16] C. Korte, M.G. Dunstall, J. Deans, Onset of the Marangoni effect during condensation of ammonia–water mixtures, in: Conference on Two-Phase Flow Modelling and Experimentation, Pisa, 1999, pp. 405–410.

[17] C. Korte, J. Deans, M.G. Dunstall, Onset of the Marangoni effect during condensation of ammonia–water mixtures—effect of temperature driving force variation, in: 3rd European Thermal Sciences Conference, Pisa, 2000, pp. 905–910.

[18] J.N.A. Morrison, The condensation of ammonia–water vapours on a horizontal tube, Ph.D. thesis, University of Auckland, New Zealand, 1996.

[19] T. Vemura, Properties of coolant-absorber systems used for absorption refrigerators, Refrigeration 52 (1977) 500–510.

[20] K. Lucas, Methods for Calculating the Properties of Materials, VDI Heat Atlas, VDI Verlag, Düsseldorf, 1993.

[21] M. Goto, T. Fujii, Film condensation of binary refrigerant vapours on a horizontal tube, in: Proc. 7th IHTC, vol. 5, 1982, pp. 71–76.

[22] P.E. Liley, R.C. Reid, E. Buck, Physical and Chemical Data, Perry's Chemical Engineers' Handbook, McGraw-Hill, New York, 1984.

[23] R. Tillner-Roth, D.G. Friend, J. Phys. Chem. Ref. Data 27 (1998) 63–96.

[24] A. Pruß, W. Wagner, in: VDI-Fortschrittsberichte, vol. 6, VDI-Verlag, Dusseldorf, 1995, p. 320.

[25] R. Tillner-Roth, 20th DKV Tagung, Heidelberg, Germany, vol. 2, 1993, 167–181.